

AD-A100 132

NEW ENGLAND RESEARCH CENTER INC SUDBURY MA
2.06 MICROMETER WIDE BANDWIDTH DETECTOR ASSEMBLY.(U)
FEB 81 A TRAINITO

F/6 17/8

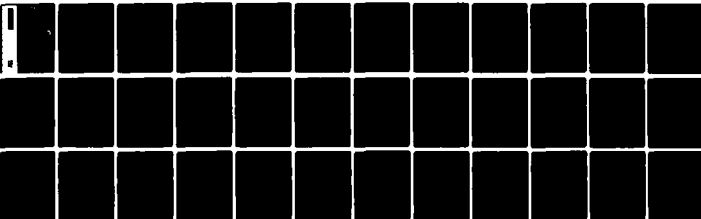
DAAK70-60-C-0009

UNCLASSIFIED

SBIE-AD-E450 005

NL

1 of 1
AD-A100 132



END

DATE

FILMED

7-81

DTIC

AD A100132

LEVEL III

AD-E450005

2

SCIENTIFIC & TECHNICAL

FINAL REPORT

FOR

"2.06 μ m WIDE BANDWIDTH DETECTOR ASSEMBLY"

DTIC
ELECTE
JUN 3 1981
S D C

February 1981

Contract No. DAAK70-80-C-0009 NEW

Prepared For

US Army Electronics Research and Development Command
Night Vision and Electro Optics Laboratory
Fort Belvoir, Virginia 22060

DISTRIBUTION STATEMENT A

Approved for public release;
Distribution Unlimited

NE
RC

81 5 07 047

(2)

**SCIENTIFIC & TECHNICAL
FINAL REPORT
FOR
"2.06 μ m WIDE BANDWIDTH DETECTOR ASSEMBLY"**

Prepared By
Angelo Trainito
NEW ENGLAND RESEARCH CENTER, INC.
MINUTEMAN DRIVE/LONGFELLOW CENTER
SUDBURY, MASSACHUSETTS 01776

February 1981

Prepared For
US Army Electronics Research and Development Command
Night Vision and Electro Optics Laboratory
Fort Belvoir, Virginia 22060

Contract No. DAAK70-80-C-0009

DISTRIBUTION STATEMENT A
Approved for public release;
Distribution Unlimited

9/2

TABLE OF CONTENTS

INTRODUCTION	1
MATERIAL OPTIMIZATION AND SELECTION	2
DETECTOR PROCESSING	3
PREAMPLIFIER CONSIDERATIONS	4
DETECTOR CONFIGURATION	9
DETECTOR PERFORMANCE	13
CONCLUSIONS AND RECOMMENDATIONS	31

Accession For	
NTIS GSA&I	<input checked="" type="checkbox"/>
DTIC TAB	<input type="checkbox"/>
Unannounced	<input type="checkbox"/>
Justification <i>per</i>	
<i>F1-182 on file</i>	
By _____	
Distribution/	
Availability Codes	
Avail and/or	
Dist	Special
<i>A</i>	

LIST OF FIGURES

FIGURE 1	Amplifier Gain vs Frequency Capacitance	6
FIGURE 2	Equivalent Circuit	8
FIGURE 3	T.E. Cooled Detector Assembly	10
FIGURE 4	Transmission Sapphire Window	11
FIGURE 5	Detectivity vs Temperature	14
FIGURE 6	Test Set-Up	17
FIGURE 7	Gain vs Frequency Amplifier S/N's 9265/9972	18
FIGURE 8	Gain vs Frequency Amplifier S/N's 9266/9973	19
FIGURE 9	Noise Measurement of NERC S/N 3274-3	21
FIGURE 10	Noise Measurement of NERC S/N 3274-5 A & B	22
FIGURE 11	Spectral Response Curves	28
FIGURE 12	Spectral Response Curves	29

LIST OF TABLES

TABLE 1 - Detector Performance	15
TABLE 2 - Test Data	24
TABLE 3 - Test Data	26
TABLE 4 - Blackbody to λ_{peak} Conversion Factor	30

ABSTRACT

This program demonstrated that high performance, wide bandwidth mercury cadmium telluride photoconductor detectors can be fabricated with a spectral peak at 2.06 micrometers. Detectivity at a frequency of 10 Megahertz are on the order of 2×10^{11} to $7 \times 10^{11} \text{cmHz}^{1/2}/\text{W}^{-1}$ at an operating temperature of 235 degrees Kelvin. This performance was achieved using standard procedures for processing 10 micron thick mercury cadmium telluride detectors.

INTRODUCTION

This final Report was prepared by New England Research Center, Inc., Minuteman Drive, Longfellow Center, Sudbury, Massachusetts, on US Army Electronics Research and Development Command, Night Vision and Electro Optics Laboratory Procurement Instrument ID Number DAAK-70-80-C-0009.

This report describes the results of a 12 month detector engineering development program leading to significant performance improvements in the mercury cadmium telluride detector which will be used in the RPV Laser Range Finder operating at the 2.06 micrometer wavelength of the HO: ULF (Holium: Yttrium Lithium Fluoride) laser.

This program was monitored by Mr. Michael Hacskeylo, Contracting Office's Representative, Night Vision and Electro Optics Laboratory, Fort Belvoir, Virginia.

The program, conducted at New England Research Center, Inc., was under the general direction of Angelo Trainito, Program Manager. He was assisted by Dr. R. Martineau, Dr. J. Miles, B. Pierson, L. MacDonald and M. Moy as prime contributors.

The detector is of mercury cadmium telluride (HgCdTe) material sensitive to the 2.06 μ m micron spectral range operating in the photo conductive (PC) mode. The design goal was to develop a process for fabricating 4 μ m thick detectors with a detectivity of $3.0 \times 10^{10} \text{ cmHz}^{1/2}/\text{W}$ at a frequency of 10MHz and a temperature of 235°K (Thermal-Electric Heat Pump). This design goal exceeds the performance of the previously reported NERC detectors by a factor of 10.

The sensitivity improvement is based on material and device processing optimization. No change is made in detector dimensions, packaging design and operating temperature. The optimized detector assemblies are readily integrable in the present RPV system.

The detectors delivered as a results of this program have a minimum spectral detectivity at $2.06\mu\text{m}$ of greater than $2 \times 10^{11} \text{cmHz}^{1/2}/\text{w}$ operating at 10 megahertz frequency and a temperature of 235°K . This performance was achieved with detectors of $10\mu\text{m}$ thick.

In order to achieve the improved detectivity performance, it was necessary to grow Mercury Cadmium Telluride crystals with a mole fraction of .475 and a majority carrier concentration of less than $1 \times 10^{14} \text{cm}^{-3}$. The crystal grown specifically for this program had a mole fraction of .472 and a carrier concentration at 77°K of $2 \times 10^{14} \text{cm}^{-3}$.

This report discusses the accomplishments along with the problems which remain to be solved. Where possible, specific recommendations are outlined to resolve these questionable areas.

Material Optimization and Selection

The theoretical performance limitations of $2.06\mu\text{m}$ wide bandwidth detectors is set by the carrier concentration. The means to achieve optimum $2.06\mu\text{m}$ performance was to grow material having a carrier concentration of $1 \times 10^{14} \text{cm}^{-3}$.

Material was grown at NERC's facility and evaluated during the early phases of this program. The ingot identified as QA48 yielded a carrier concentration of $2 \times 10^{14} \text{cm}^{-3}$.

During crystal growth, the pressure vessel burst. A visual examination of this ingot revealed a high density of second phase distributed throughout most of the ingot. The inclusions are concentrated most heavily in the central portion of the material and

decreases toward the periphery of the ingot where some useable material was found. The nature of the second phase was thought to be from an excess of tellurium which formed during the reaction/solidification stage due to uncertainties in the constitution of the vapor phase. This was confirmed by energy dispersive x-ray spectroscopy (EDXS) studies.

Because of the above conditions only a small amount of ingot is usable. The electrical properties of the usable portion of the crystal, however, are very encouraging. The characteristics at 77°K of this material are:

Carrier concentration (N_0).....	$2 \times 10^{14} \text{cm}^{-3}$
Mobility (μ).....	$1.27 \times 10^3 \text{cm}^2 \text{V}^{-1} \text{s}^{-1}$
Resistivity (ρ).....	48.1 Ωcm
Mole Fraction (x).....	.472

Detector Processing

The thickness, 4 microns, of the detector was one of the major features required to meet the performance requirements of this program. Several changes in the standard processing techniques were made to process 4 ± 0.5 micron thick detectors. Glue line thickness, that is, the adhesive between the HgCdTe material and the substrate, was one of the major problems in achieving a $4 \pm .5$ microns thick wafer. A glue line to within 1 micron over the entire wafer surface, approximately 12mm in diameter, was found impractical within the limitations of this program.

Detectors of standard thickness, 10 microns, were fabricated and tested. Detectors with acceptable performance were selected to be reduced to $4\mu\text{m}$ in thickness using ion beam milling techniques with a post etch process to remove surface damage. The post ion beam milling tests showed a reduction in detector performance. More experiments are required to optimize this procedure for use as a method of reducing the thickness of detectors.

It was decided to process individual detectors on .100 square substrate. This attempt was tedious and costly. Performance of the 4 μ m thick detectors which reached test were inferior to detectors processed using the standard method and standard thickness (10 microns).

Since the detectors made from ingot QA48 using the standard method (detector thickness of 10 microns) exceeded the design goal performance requirements, it was decided to select two for the assemblies.

Preamplifier Considerations

A preamplifier (Model 070/40) and a frequency boosting amplifier (Model 608) purchased from Perry Amplifier are supplied with each detector unit. The complete wide bandwidth detector assembly is compatible to the RPV-system. The special frequency boosting amplifier increases the signal at frequencies above the detector knee ($1/2\pi\tau_{eff}$). Some consequence and precaution in the use of the current mode amplifier selected for this assembly are discussed below.

The basic challenge with the signal processing electronics is high frequency considerations for low frequency detectors. All photoconductive IR detector can be successfully operating in either current or voltage mode. The photoconductor is limited to its photon response time in both the voltage and current mode. Operating a photoconductor in the current mode will not increase the response time of the detector. It can aid in the neutralization of the input amplifier capacitance factor which may or may not be a significant bandpass limiting factor. Bandwidth expansion of photoconductive response is best served by use of a secondary peaking amplifier which will supply extra gain (6db/Octave) to the overall detector preamplifier bandpass. This nonlinear amplifier gain characteristic

can be tailored to effectively linearize the detector output to most any reasonable bandwidth. The preamplifier requirements in such a system demand that its fundamental bandwidth be in excess of the system bandwidth requirements. The relationship of gain versus frequency as a function of the peaking capacitor is shown in Figure 1.

The addition of a peaking amplifier to extend response bandwidth is not without penalty. The power noise bandwidth of the peaking amplifier is fundamentally higher than linear bandpass amplifiers.

The operating characteristics of all feedback amplifiers are dependent upon the impedance of the driving source. A pure resistive source impedance generally gives predictable operating results and best realizes the full bandwidth, noise and linearity characteristics of the amplifier. The pure resistive source impedance, however, is a special case. In most cases, the source impedance characteristic includes a reactive component X_C which represents the capacitive component of the source. This reactance is due to both mechanical (cables, etc..) and intrinsic source capacitance considerations. The effect of this input capacitance is a function of frequency and may range from negligible to major consequence (instability).

The presence of input capacitance introduces phase shift into the loop. The amount of phase shift is dependent upon the amplifier bandpass and the magnitude of input capacitance. This phase shift will generate the classic "ringing effect" and a contraction in overall bandwidth. These effects are especially troublesome in wide-band applications. Installation of proper reactive compensation in the amplifier feedback loop can minimize the ringing effect to negligible levels. The bandwidth of the amplifier, however (assuming the same feedback resistance), will contract in proportion to the feedback compensation. Feedback compensation can be added to all amplifiers to minimize input capacitance effect.

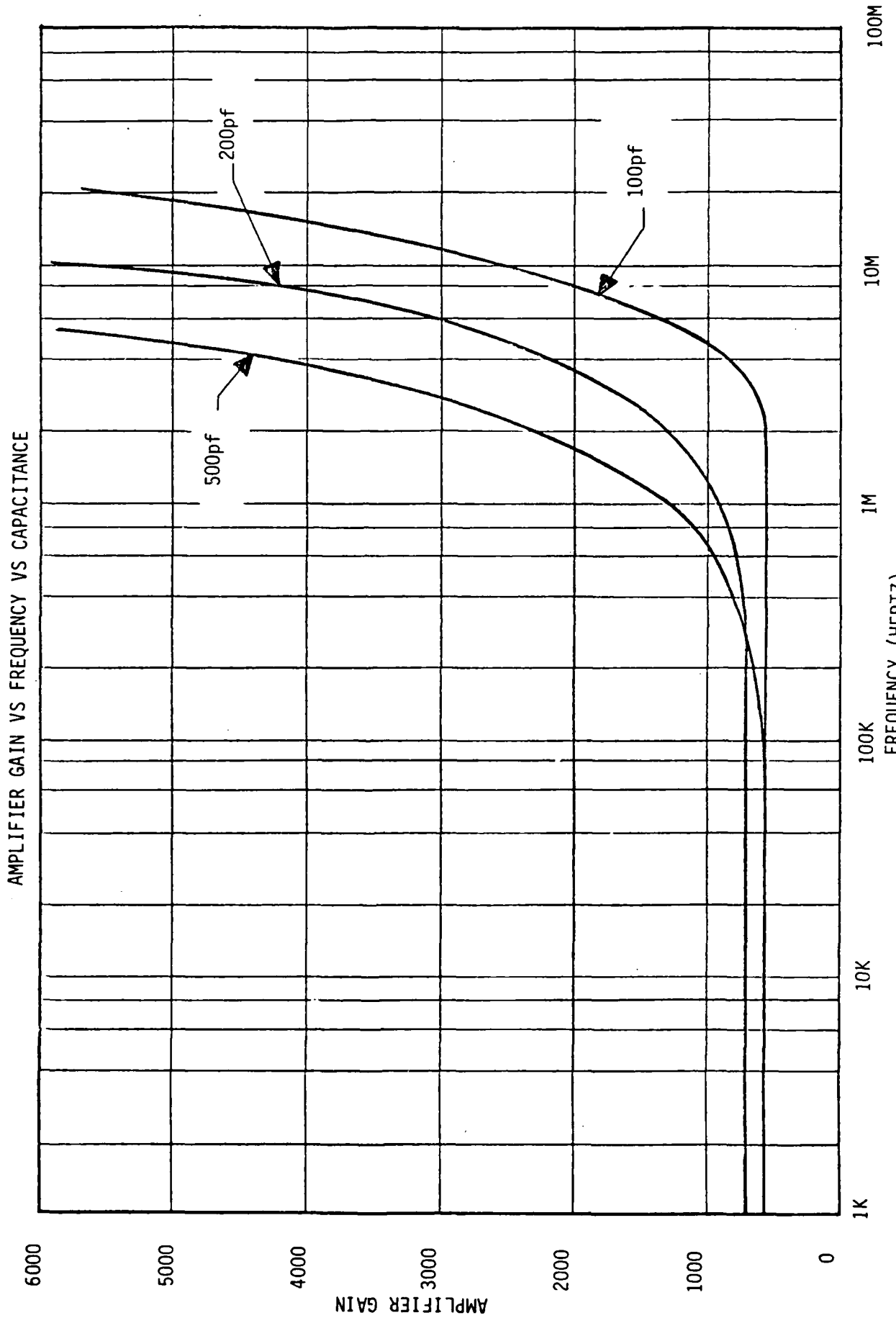


FIGURE 1

The effect of input capacitance to the overall noise performance of a feedback amplifier is well established. A full analysis of the phenomenon is not readily found and is at best overly complicated. A simple analysis utilizing classic feedback criterion best illustrates the problem. An equivalent circuit and noise analysis are illustrated in Figure 2.

The analysis is based on the following simplifying assumptions:

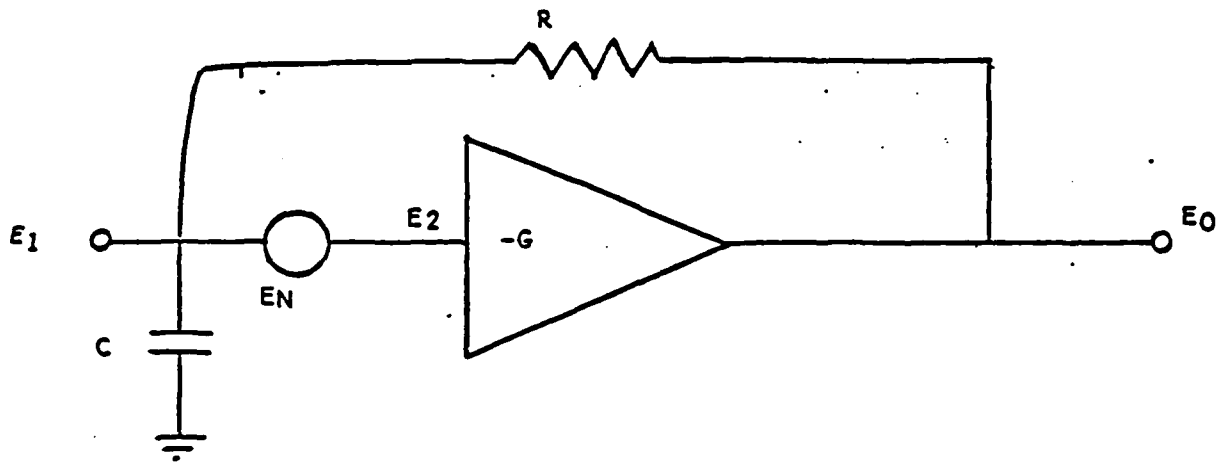
1. Amplifier bandwidth is flat from DC to infinite frequency.
2. Source resistance is infinite.
3. Source noise is neglected.
4. All the noise is generated by the amplifier and can be lumped into a single equivalent white noise generator referred to the input.

It can be seen that the addition of capacitance across the input increases the noise level at the higher frequencies (with a resulting increase in noise figure). This will occur even though the noise figure of the amplifier open loop is essentially zero. It is not attributable to a poor noise figure of the amplifier.

In the actual case, bandwidth limitations of the amplifier and noise spectrum prevent the noise level increase from approaching the theoretical $20 \log DB$ (which can be a very large number). We can however expect to see a significant increase in the noise level as the capacitance is introduced. This has been verified experimentally in the laboratory. The capacitance noise effect indicates that input capacitance must be kept at an absolute minimum if the best noise performance of the amplifier is to be realized.

Another source of noise external to the intrinsic noise of the amplifier is the thermal noise introduced to the input of the amplifier by the feedback resistor. The noise performance of the amplifier will be a function of this resistance and its value must be calculated into the amplifiers noise figure equations as an external noise source.

EQUIVALENT CIRCUIT



NOISE ANALYSIS

$$E2 = \frac{(1/SC)E0}{(1/SC)+R}$$

$$+EN = -(1/G)E0$$

EN = AMPLIFIER NOISE
REFERRED TO INPUT

$$EN = E0 \left(\frac{1}{1+SCR} + \frac{1}{G} \right)$$

$$E0 = \frac{EN(1+ST)}{1+(1/G)+(ST/G)} = \frac{EN(1+ST)}{1+ST'}$$

WHERE $T' = T/G = RC/G$

WITH C (CAPACITANCE)

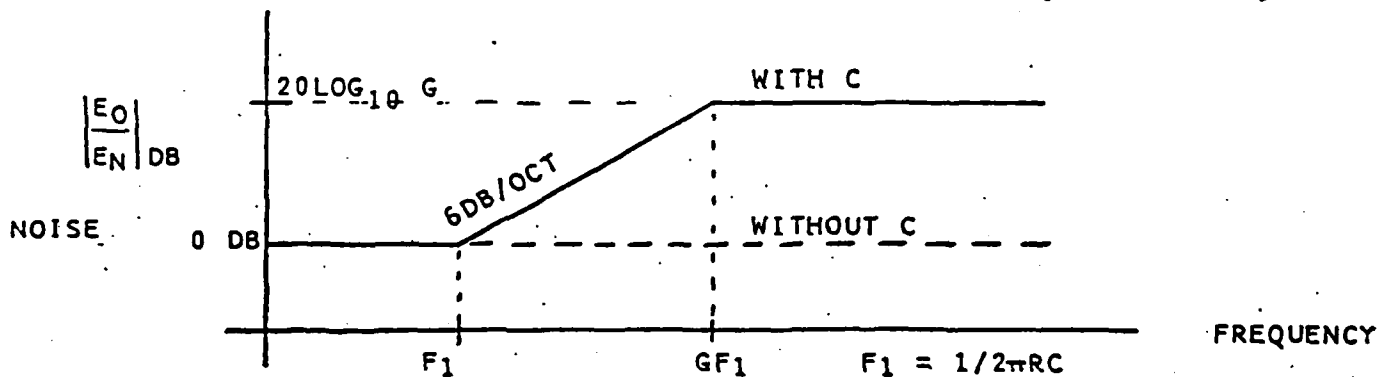


FIGURE 2

It follows the maximum noise performance will be realized when the feedback resistance is maintained at a value much greater than the driving source impedance. A source to feedback ratio of 1:10 will give rise to 1DB of extraneous feedback thermal noise, which for most case is an acceptable noise loss.

Considerable consideration was given to the selection and design of the preamplifier and the frequency boosting amplifier. The present design represents the best signal processing electronics one can expect to use with low noise detectors. Because of the noise limitations of such an amplifier design, detector noise at 10 Mega-hertz was not observable. Therefore, the effective D^* at the corner frequency (f^*) is lower than $D^*(0)$.

Detector Configuration

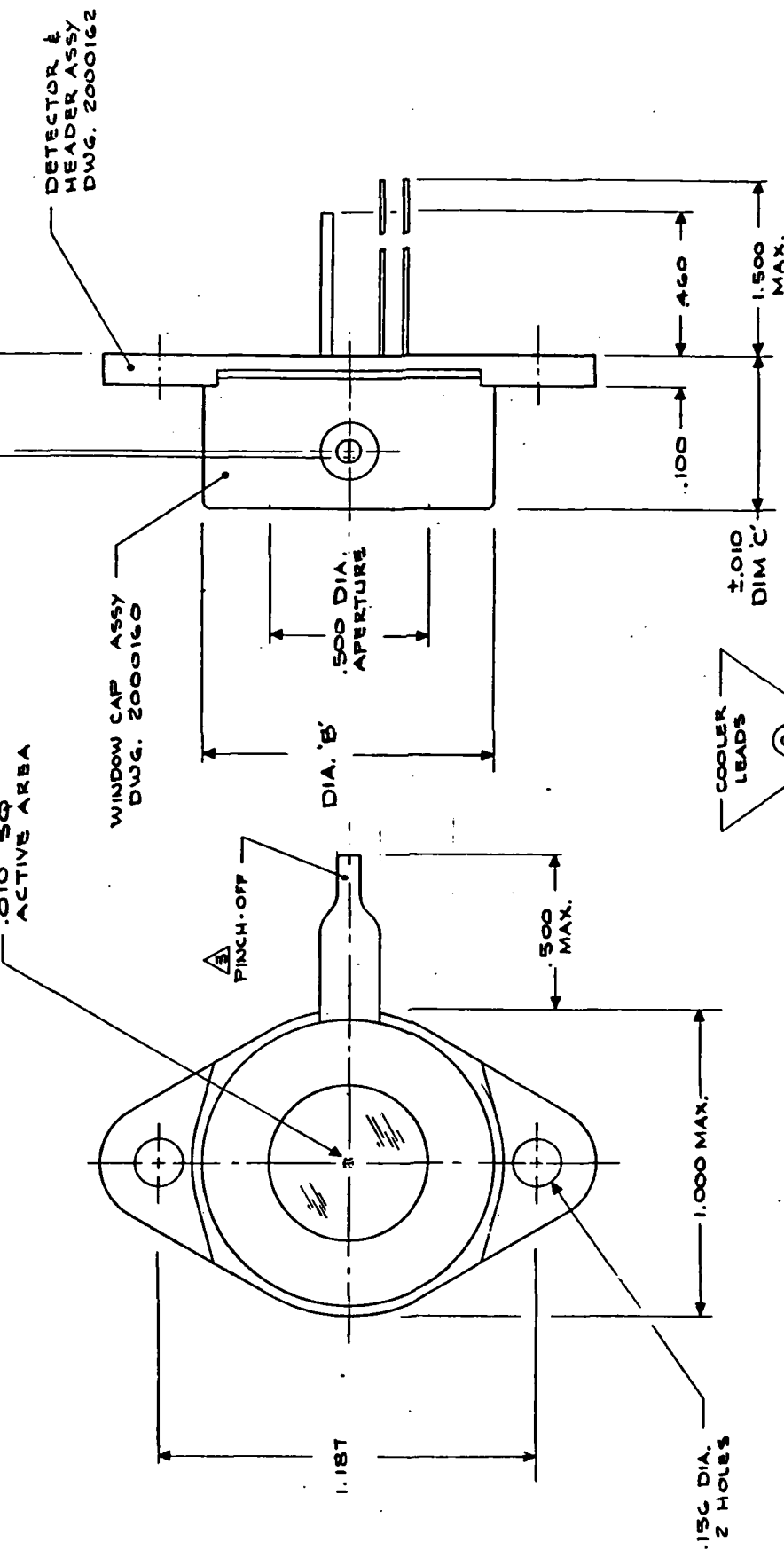
Two Mercury Cadmium Telluride detectors delivered on this contract were housed in a T0-18 header assembly. TE cooler detector assembly Drawing 2000163, reprinted as figure 3, shows the final assembly. This section will verbally describe the units from the radiation entrance window to the output terminal.

Unit serial number 3274-3 was equipped with an Infrared Industries Inc. supplied sapphire window. The window was antireflection coated on both sides. The transmission spectra is shown in figure 4. At $2.06\mu\text{m}$ the window transmission is on the order of 99%.

The window is mounted in a T0-18 cap supplied by Marlow Industries. The epoxy used to seal the window is Armstrong A-12. The cap is also sealed to the T0-18 header with this epoxy. The copper pinch of tubulation is soldered into the cap using 60/40 lead tin solder.

NOTES:

1. ACTIVE AREA TO BE CONCENTRIC TO HEADER &'S TO WITHIN .010 TIR.
2. ASSEMBLY TO BE VACUUM TIGHT TO 10^{-10} ATM CC/SEC OF He WHEN TESTED ON A MASS SPECTROMETER.
3. PINCH-OFF AT 10^{-7} TORR OR LOWER.
4. THIS ASSEMBLY TO MEET ALL REQUIREMENTS OF CONTRACT 3274 AV.



	DIM 'A'	DIA 'B'	DIM 'C'
2 STAGE COOLER	.342	.925	.525
4 "	.492	1.000	.675

REAR VIEW
PIN DESIGNATIONS

DETECTOR LEADS

THERMISTOR LEADS

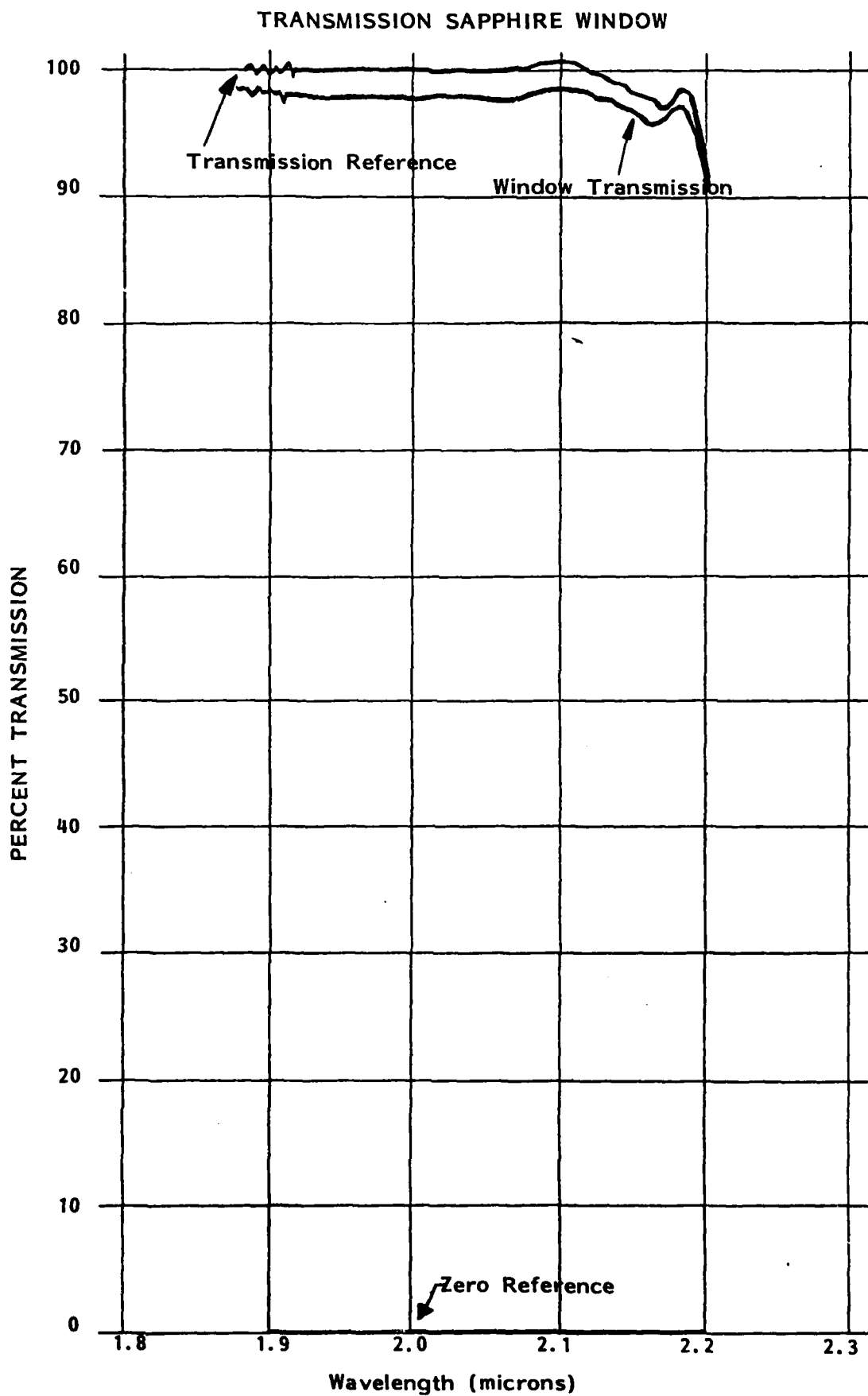
COOLER LEADS

DETECTOR & HEADER ASSY DWG. 2000162

NEW ENGLAND RESEARCH CENTER, INC.			
1000 W. 10TH AVE. / LOWELL, MASS. 01860			
DATE: 4/1	DESIGNED BY: PLO 3	APPROVED BY: P. DEJANUE	SCALE: 1/1
T.E. COOLED DETECTOR ASSY			2000163

NOTE: TABLE ADDED FOR THE CONVENIENCE OF THIS REPORT. DRAWING HAS NOT BEEN REVISED

FIGURE-3



The detector active area .010 x .010 inches and 10 microns thick is mounted on a Marlow Industries thermo electric heat pump model MI 2021 designed for operation at 233°K. The heat pump was supplied with a thermistor model MI-T-1.25K. The heat pump, T0-3 header and power terminals were soldered to the T0-18 header by Marlow Industries. The output of the detector and temperature sensor (thermistor) are terminated at the 6 pin T0-3 header; two pins for the thermistor and two pins for the detector. The remaining two pins are not used. The power for the heat pump is supplied thru two individual terminals marked "(+)" and "(-)" on the back side of the header.

The T0-18 header is equipped with two mounting holes for convenient mounting to a heat sink.

The second unit serial number 3274-5 was similar in configuration to unit serial number 3274-3 with one basic difference. The heat pump was a Marlow Industries 4 stage model MI 4012T designed for operation at 195°K. The additional height of the 4 stage cooled necessitated a modification in the cap design. The distance from the backside of the window to the detector surface was maintained for both units at a nominal dimension of .183 inches. Dimensions A, B, and C shown in Figure 3 indicate the changes necessitated by the 4 stage heat pump.

As a final step in the assembly prior to placing the unit on the vacuum pump-out station, a leak tight test was performed. A leak rate of less than 10^{-10} standard cc/sec of helium was measured on a mass spectrometer.

Detector Performance

The objective of this program is the optimization of detectivity of $2.06\mu\text{m}$ (Hg,Cd)Te photoconductive detectors operating at 235°K and having a minimum bandwidth of 10 Megahertz. Specifically, the design goals are:

Det. Area	Temperature	$D^* (0) \left(\frac{\text{cmHz}^{\frac{1}{2}}}{\text{W}} \right)$	$f^*(\text{MHz})$
$(.25\text{mm})^2$	235°K	$\geq 3.0 \times 10^{10}$	10

The inprocess test results of at least 8 detectors indicated that substantial performance improvement is possible by reducing the operating temperature of the detector. The results of these tests are summarized in the graph shown in figure 5. The two lines represent the D^* performance range of all measured detectors at a wavelength of $2.06\mu\text{m}$ and at an operating frequency of 10KHz. Measurements were taken at 300°K , 233°K , 87°K , and 77°K . The lines drawn between 233°K and 87°K is the most probable estimate of the D^* performance over this temperature range. Based on this data it was decided that one of the two units to be delivered would be with a 4 stage cooler with a goal of achieving an operating temperature of 195°K . Data points have been made on Figure 5 showing the $D^*(\lambda_p, 100\text{KHz}, 1)$ performance for both units. The performance improvement of unit serial number 3274-5 operated at 207°K is as predicted approximately 2 times the performance measured at 233°K . A temperature of 195°K was not reached because the heat sink was not optimized for a 4 stage cooler which requires higher operating power.

The detector performance of the two units is summarized in Table 1. The design goal requirements are restated on this table for comparison to the performance obtained on the 2 units. The D^* performance of

DETECTIVITY VS TEMPERATURE

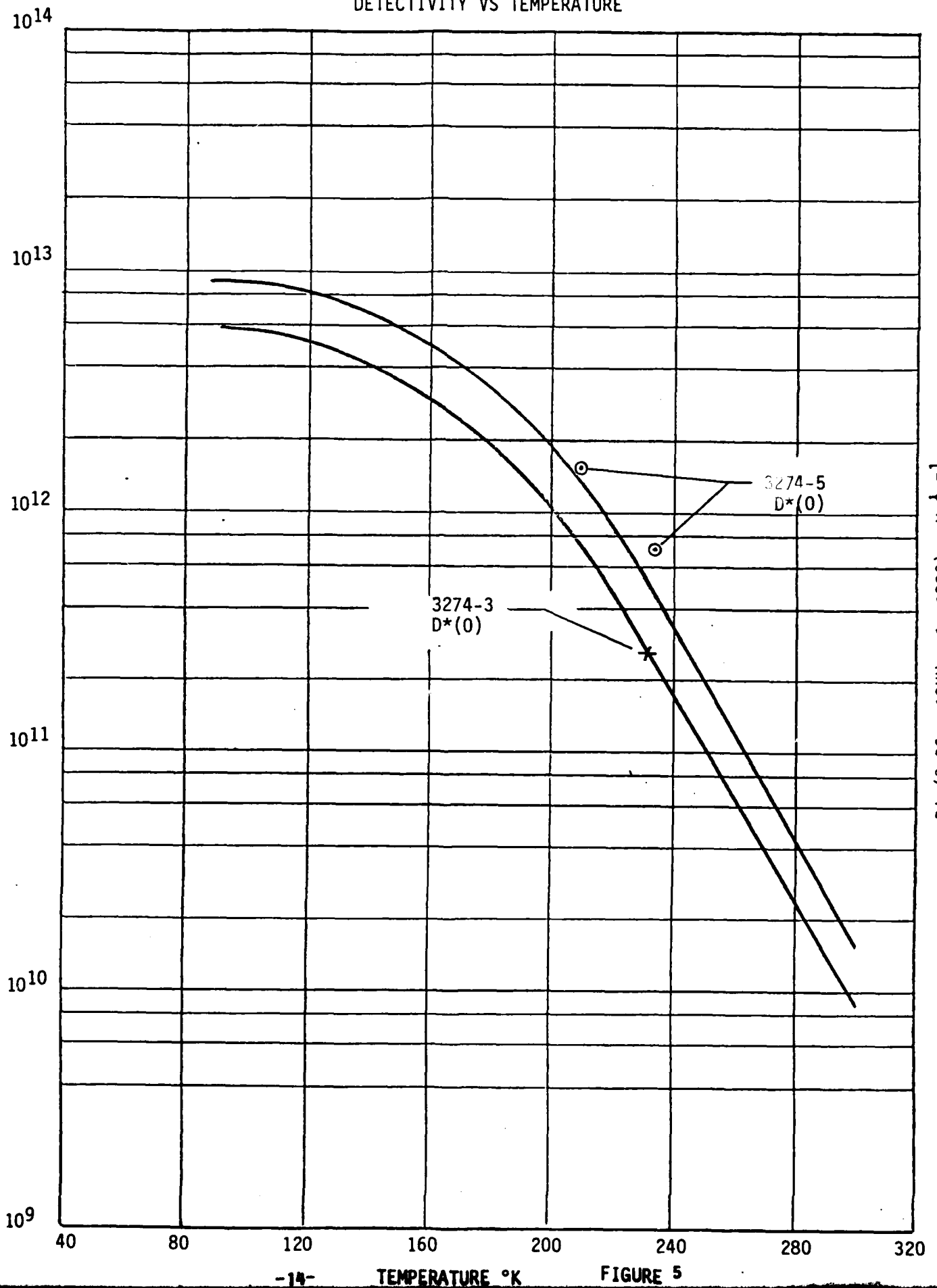


TABLE 1

DETECTOR PERFORMANCE

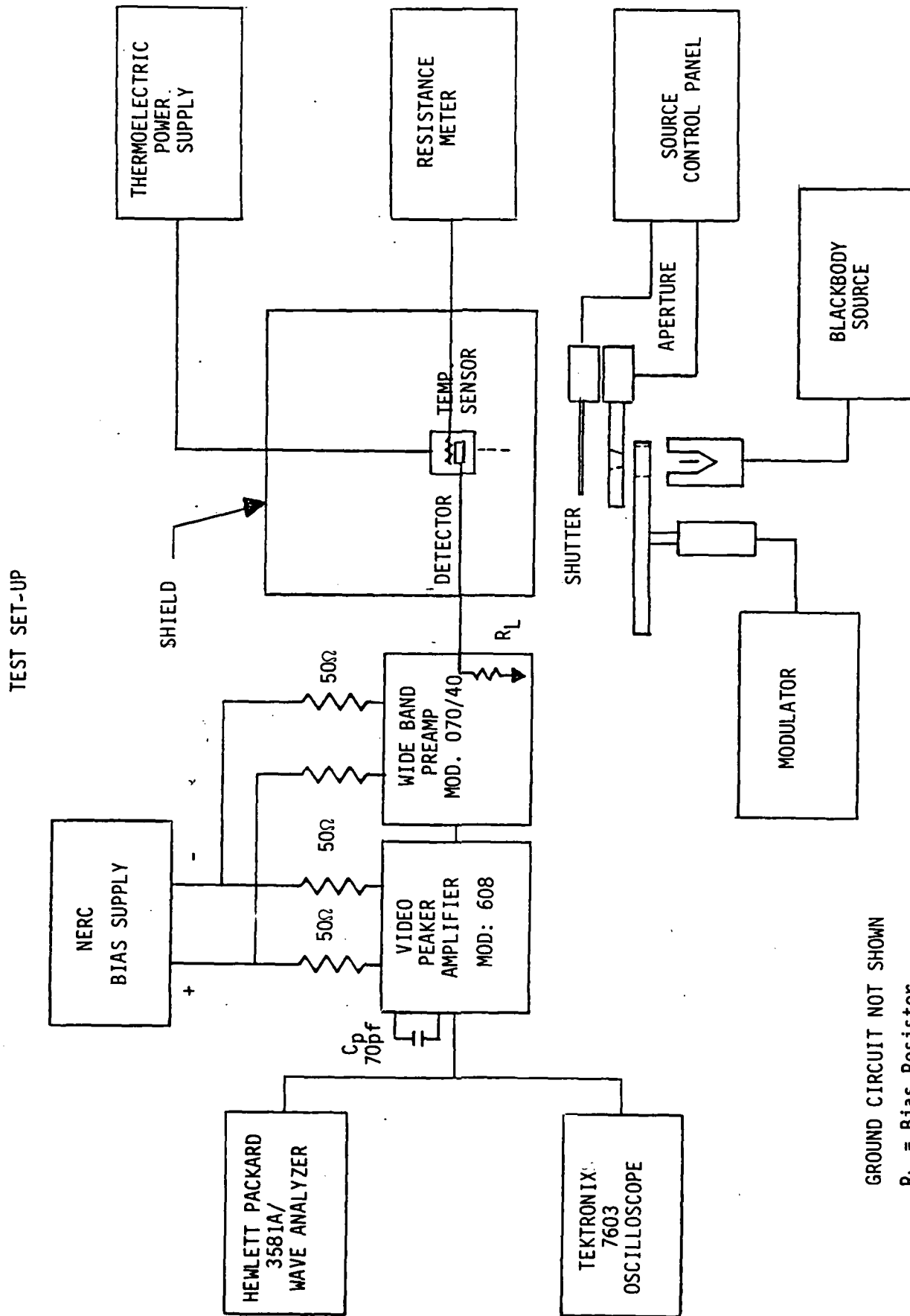
DESIGN GOAL	POWER DISSIPATION W/cm ²	TEMPERATURE °K	RESISTANCE (K Ohm)	RESPONSIVITY (2.06μm, 10MHz) Volts/Watt	NOISE DENSITY (10MHz, 1) x 10 ⁻⁹ V/Hz ^{1/2}	f* (MHz)	DETECTIVITY (2.06μm, 10MHz, 1) cm-Hz ^{1/2} /W
	>60	233	50-100	-	-	10	> 3 x 10 ¹⁰
3274-3	4.2	233	.672	21,000	218	6	2.44 x 10 ¹¹
3274-5	4.3	233	1.2	104,000	1.4	7.5	6.8 x 10 ¹¹
3274-5	4.3	207	.098	292,000	1.2	5.6	8.7 x 10 ¹¹

unit 3274-3 at 233°K is almost an order of magnitude greater than the design goal. The performance of unit 3274-5 is significantly higher at a temperature of 233°K and still higher at 207°K. The stated D^* (10 MHz) is for the detector/amplifier assembly. Since, the noise at 10 MHz is predominantly amplifier noise the detector D^* is understated. The detector $D^*(2.06\mu\text{m}, 100\text{KHz}, 1)$ without the peaking amplifier, is $16.5 \times 10^{11} \text{cmHz}^{1/2}/\text{w}$ at an operating temperature of 207°K. This is approximately a factor of 2 higher than the D^* at a frequency of 10 Megahertz ($8.7 \times 10^{11} \text{cmHz}^{1/2}/\text{w}$).

It is obvious from these measurements that system performance is limited by the preamplifier/video peaking amplifier as the operating temperature of the detector decreases below 233°K.

The block diagram of figure 6 shows the set-up used to measure the performance of the detectors. The procedure followed the below sequence:

1. Measure performance vs bias to determine optimum bias current. The video peaking amplifier was not used for this series of test, measurements were taken at the output of the wideband preamplifier at a frequency of 50K Hertz for noise and 1K Hertz for signal.
2. The bias resistor (R_L) was selected and soldered to the wideband preamplifier.
3. The gain of the wide bandwidth preamplifier was taken as a function of frequency out to 18 megahertz (see figures 7 and 8).
4. The noise vs frequency of the detector was measured at operating temperature from 1K hertz to 18 megahertz.



GROUND CIRCUIT NOT SHOWN

R_L = Bias Resistor

C_p = Peaking Capacitor

SHUTTER - OPEN FOR SIGNAL MEASUREMENTS

VOLTMETER - OUT OF CIRCUIT FOR MEASUREMENTS

FIGURE 6

N.E.R.C. ASSEMBLY S/N 3374-3

GAIN VS FREQUENCY
AMPLIFIER S/N's 9265/9972

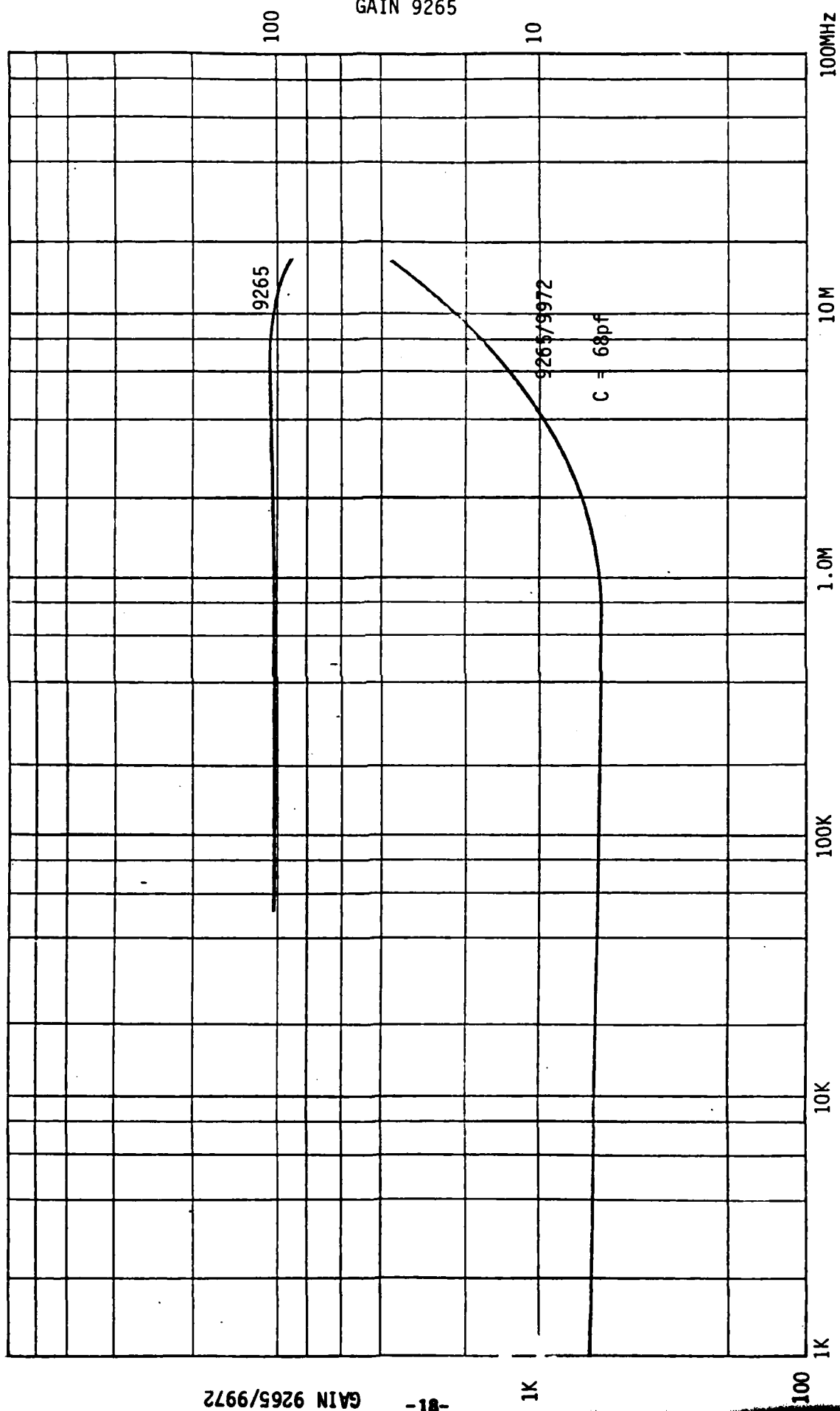
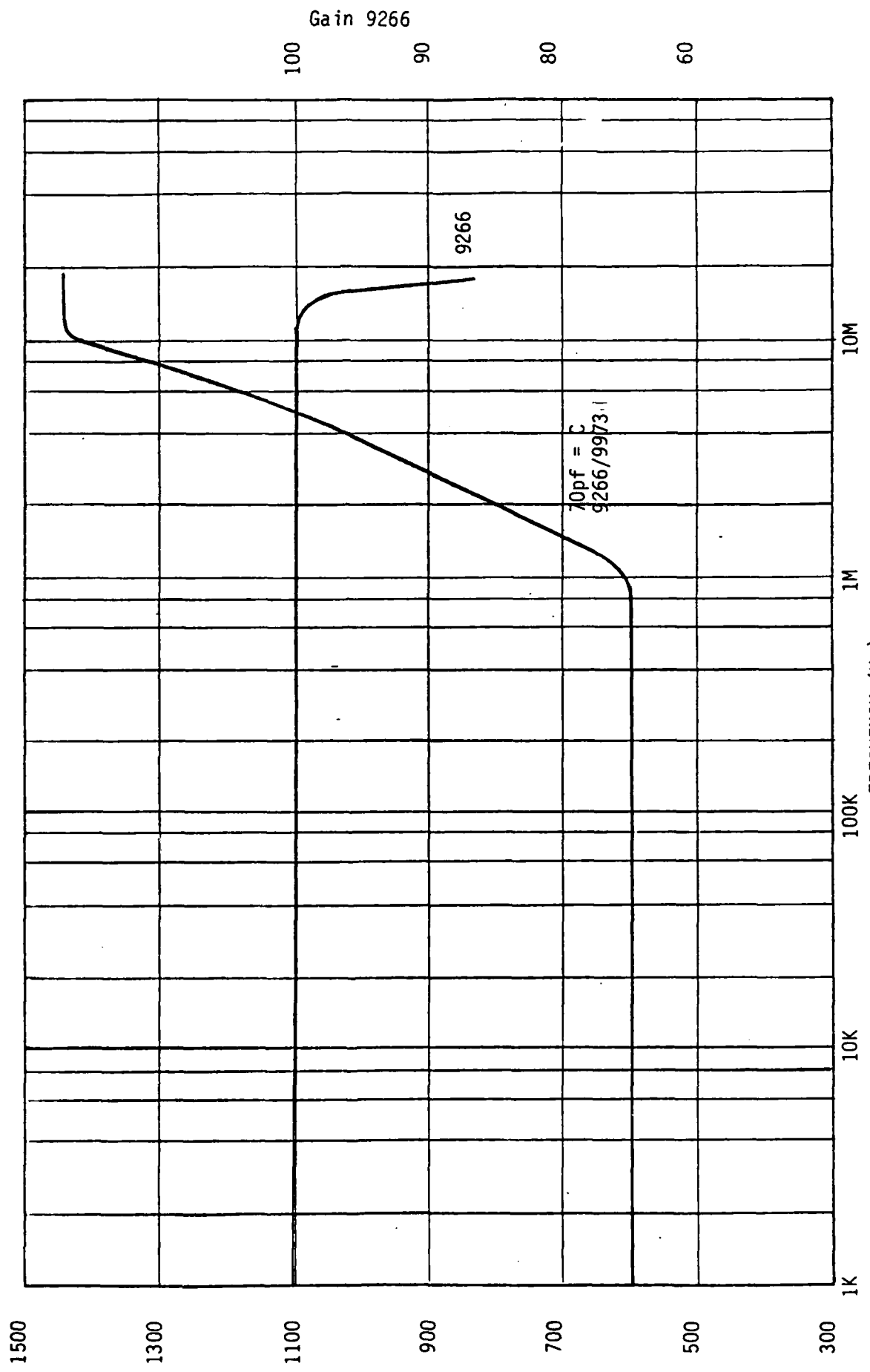


FIGURE 7

GAIN VS FREQUENCY
AMPLIFIER S/N's 9266/9973

N.E.R.C. ASSEMBLY S/N 3374-5



Gain 9266

Gain 9266/9973

FIGURE 8
FREQUENCY (Hz)

5. Noise density was calculated over the frequency band and the cut-off frequency determined. See figures 9 and 10 (A & B) respectively for S/N 3274-3 and S/N 3274-5 noise density performance.
6. The noise was then measured between 100KHz and 10MHz the output of the video peaking amplifier. The peaking capacitance was adjusted until signal and noise characteristics at the output of the amplifier system was flat over a wide bandwidth of frequencies without drastic changes in the G-R noise characteristics of the detector. (See figures 9 & 10).
7. Once the peaking capacitance was established, the gain of the system was measured. A plot of the system gain is given in Figures 7 and 8.
8. The final measurement taken was the detector signal at 1kHz.
9. The spectral response of the detector was measured with a Digilab FTS-15 spectrophotometer.
10. Responsivity, noise density and detectivity calculations were then made.

The test conditions and results of the measurements recorded for each unit are listed in Table 2 and 3 with the spectral response curves shown in Figures 11 and 12.

The conversion factor "G", from blackbody to peak wavelength is calculated in Table 4.

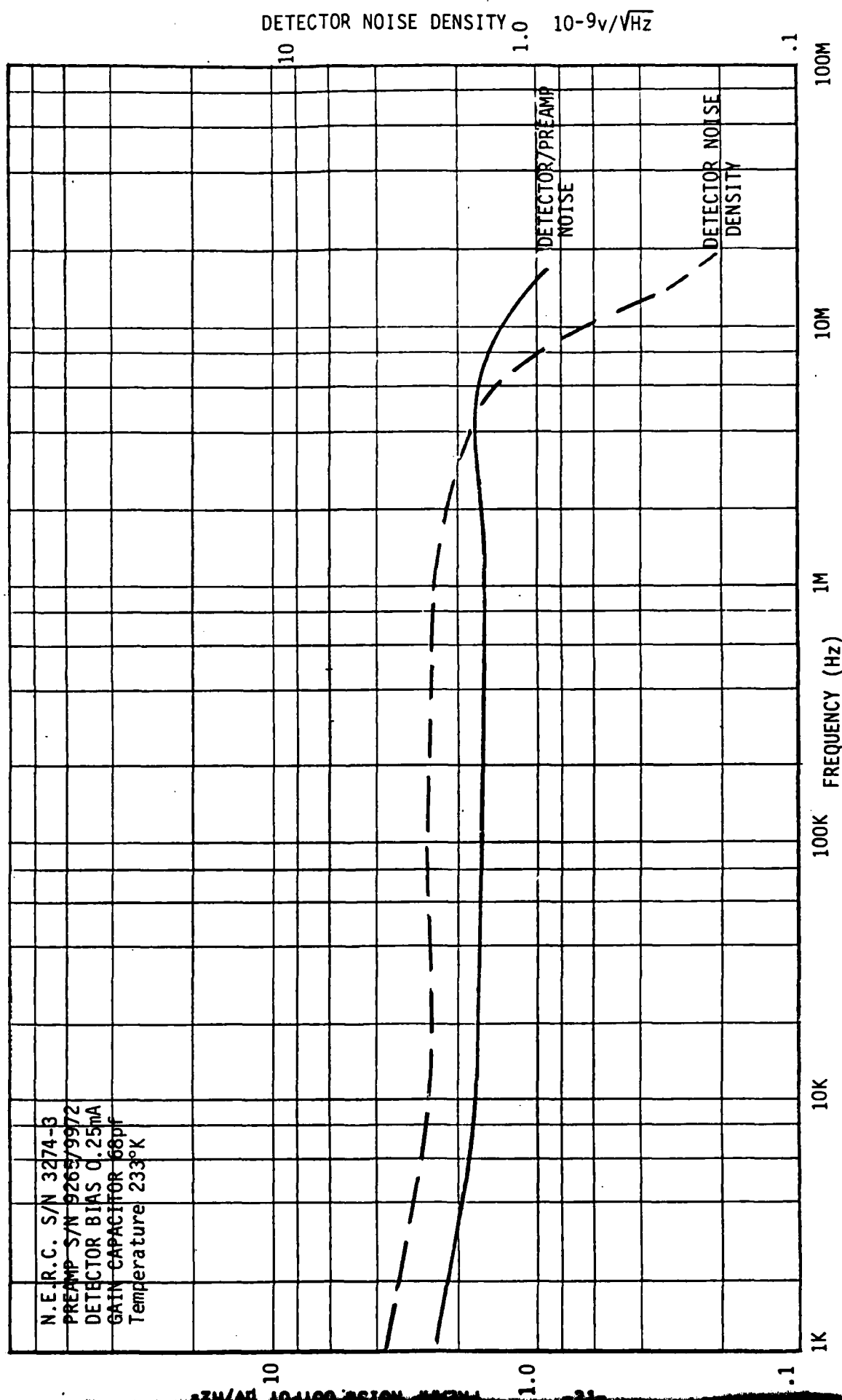
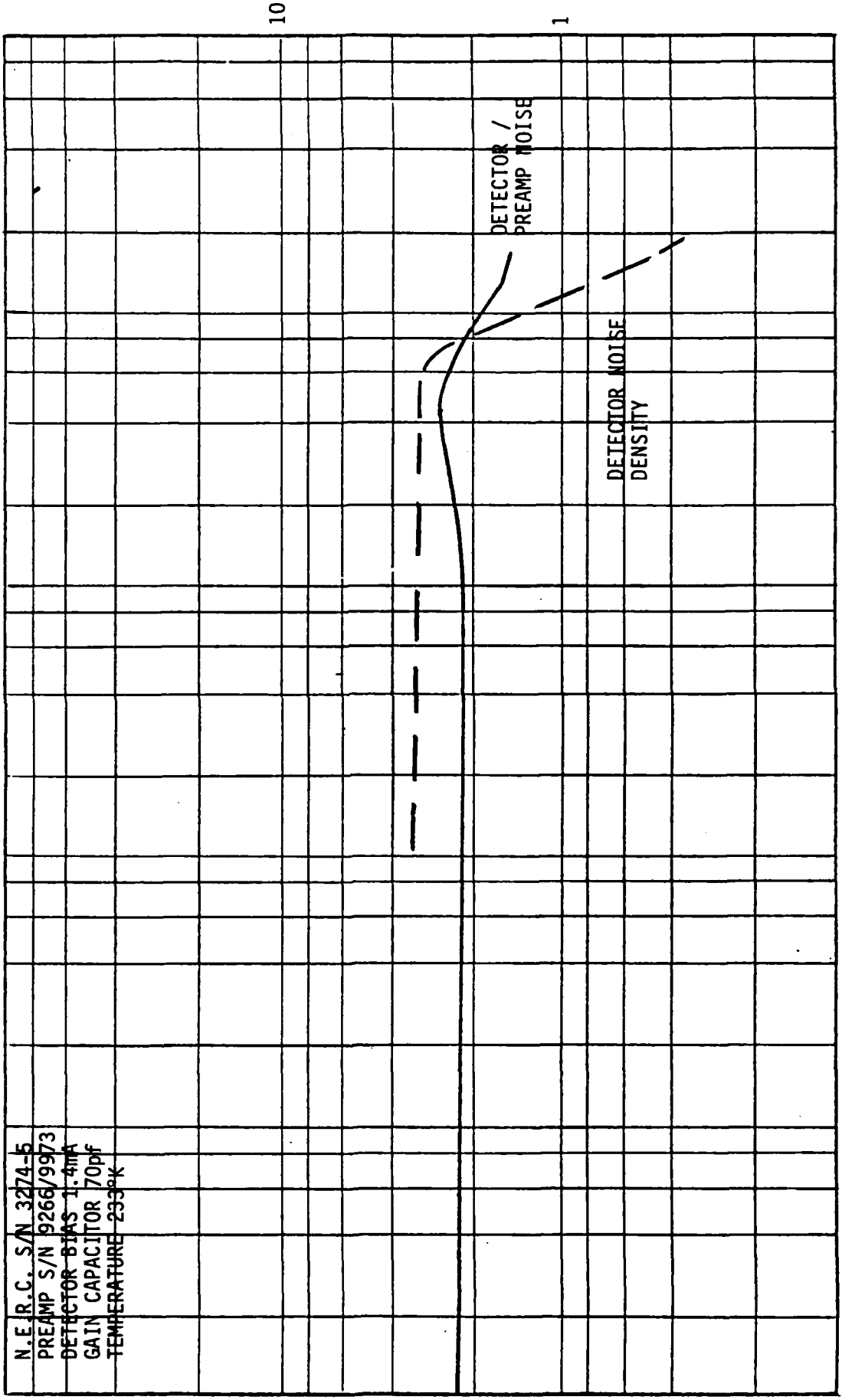
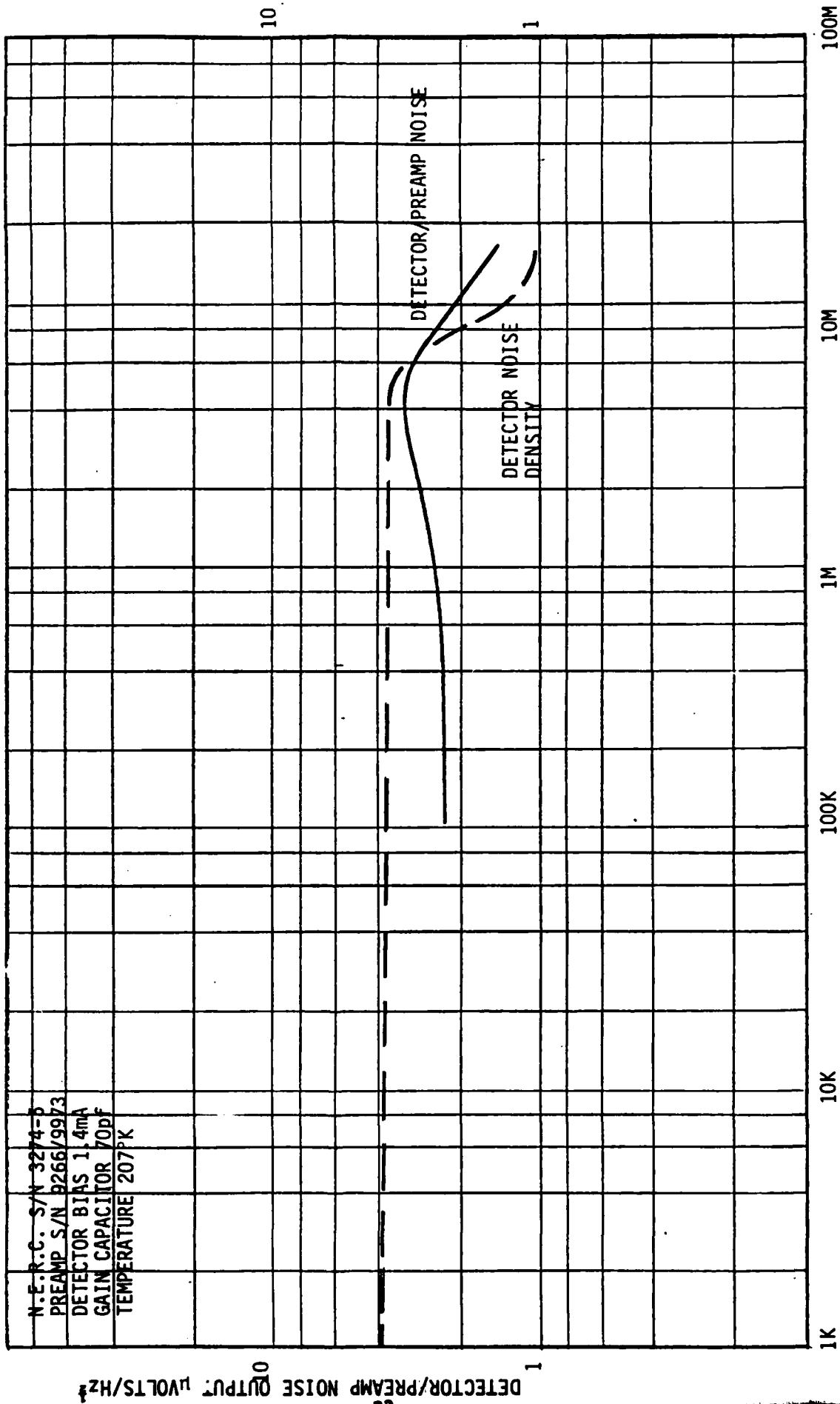


FIGURE 9

N.E.R.C. S/N 3274-5
 PREAMP S/N 9266/9973
 DETECTOR BIAS 1.4mA
 GAIN CAPACITOR 70pf
 TEMPERATURE 233°K



FREQUENCY HZ
 FIGURE 10A



FREQUENCY HZ
 FIGURE 10B

TABLE 2

NERC JOB #3274

CUSTOMER: NVL P.O.# DAAK70-80-C-0009

2.06 μ m WIDEBAND DETECTOR ASSEMBLY

TEST DATA

S/N 3274-3

MODEL NO.....	2000163
DETECTOR ID.....	48-528-3
T.E. COOLER NO.....	001
DETECTOR ELEMENT SIZE.....	.010 x .010 INCHES
DETECTOR THICKNESS.....	10 MICRONS
OPERATING TEMPERATURE.....	233°K
BACKGROUND TEMPERATURE.....	300°K
BLACKBODY TEMPERATURE.....	1000°K
APERTURE DIAMETER.....	.211cm
CHOPPER RMS FACTOR.....	.36
DETECTOR-TO -APERTURE DISTANCE.....	34cm
NOISE BANDWIDTH.....	200Hz
AMPLIFIER GAIN 100KHz.....	615
10MHz.....	2000
PEAKING AMPLIFIER CAPACITANCE	68pf
WAVELENGTH CUTOFF.....	2.2 μ
WAVELENGTH PEAK	2.05 μ

S/N 3274-3
2.06 μ m WIDEBAND DETECTOR ASSEMBLY

TEST DATA
TABLE 2 (continued)

RESISTANCE.....	672 Ohms
LOAD RESISTOR.....	51K Ohms
BIAS VOLTAGE.....	+12V DC
SIGNAL (1000Hz).....	14mv
NOISE (100KHz).....	23 μ v
(10MHz).....	19 μ v
"G" FACTOR.....	11.9
RESPONSIVITY (R_{BB}).....	1765 v/w
($R_{\lambda p}$).....	21002 v/w
NOISE DENSITY (N_1 100KHz).....	2.64×10^{-9}
(N_1 10MHz).....	2.18×10^{-9}
DETECTIVITY (D^*_{BB} , 10KHz, 1).....	$17.0 \times 10^9 \text{ cmHz}^{1/2}/\text{w-1}$
(D^* 2.06, 100KHz, 1).....	2.02×10^{11} " "
(D^* 2.06, 10MHz, 1).....	2.44×10^{11} " "

$$D^*(2.06, 10\text{MHz}, 1) = \frac{N_1(10\text{MHz})}{N_1(100\text{KHz})} \cdot D^*_{2.06, 100\text{KHz}, 1}$$

COOLER POWER

.75Amps

TABLE 3

2.06 μ m WIDEBAND DETECTOR ASSEMBLY

TEST DATA
S/N 3274-5

MODEL NO.....	2000163	
DETECTOR ID.....	48-528-5	
T.E. COOLER NO.....	MI4012T	
DETECTOR ELEMENT SIZE.....	.020 x .010 INCHES	
DETECTOR THICKNESS.....	10 MICRONS	
BACKGROUND TEMPERATURE.....	300°K	
BLACKBODY TEMPERATURE.....	100°K	
APERTURE DIAMETER.....	.211cm	
CHOPPER RMS FACTOR.....	.36	
DETECTOR-TO-APERTURE DISTANCE.....	34cm	
NOISE BANDWIDTH.....	200Hz	
AMPLIFIER GAIN 100KHz.....	600	
10MHz.....	1437	
PEAKING AMPLIFIER CAPACITANCE.....	70pf	
OPERATING TEMPERATURE.....	233°K	207°K
WAVELENGTH CUTOFF (MICRONS).....	2.19	2.19
WAVELENGTH PEAK (MICRONS).....	2.08	2.08
RESISTANCE (OHMS).....	1200	976

S/N 3274-5
2.06 μ m WIDEBANDWIDTH DETECTOR ASSEMBLY

TEST DATA
TABLE 3 (continued)

	(233°K)	(207°K)
LOAD RESISTOR (K OHMS).....	7.5	7.5
BIAS VOLTAGE (VOLTS DC).....	+12	+12
SIGNAL (1000Hz) (M VOLTS).....	66	185
NOISE (100KHz) (MICRO VOLTS).....	32	38
(10MHz) (MICRO VOLTS).....	28	30
"G" FACTOR.....	11.9	11.9
RESPONSIVITY, R _{BB} (100KHz) VOLTS/WATT.....	8741	24,500
R _{λp} (100KHz) VOLTS/WATT.....	104,000	292,000
R _{λp} (10MHz) VOLTS/WATT.....	35,000	108,000
NOISE DENSITY, N. (100KHz) 10 ⁻⁹ v/Hz ^{1/2}	3.77	4.88
N. (10MHz) 10 ⁻⁹ v/Hz ^{1/2}	1.40	1.20
DETECTIVITY, D* (BB, 100KHz, 1) 10 ¹⁰ cmHz ^{1/2} /w ⁻¹	5.9	13.9
D*(2.06 μ , 100KHz, 1) 10 ¹¹ cmHz ^{1/2} /w ⁻¹	7.0	16.5
D*(2.06 μ , 10MHz, 1) 10 ¹¹ cmHz ^{1/2} /w ⁻¹	6.8	8.7
COOLER POWER (AMPS).....	.65	.75

$$\text{RESP (2.06}\mu\text{, 10MHz, 1)} = \frac{N_{(10\text{MHz})}}{N_{(100\text{KHz})}} \cdot \text{Resp (100KHz)}$$

$$D^* (2.06\mu, 10\text{MHz}, 1) = \frac{S}{N} (10\text{MHz}) \cdot \frac{S}{N} (100\text{KHz}) \cdot D^* (2.06\mu, 100\text{KHz}, 1)$$

*NOISE DENSITY IS LIMITED BY AMPLIFIER NOISE

N.E.R.C. JOB# 3274
CUSTOMER: NVL P.O.# DAAK70-80-C-0009
2.06 μ m Wide Bandwidth Detector Assembly
S/N 3274-3



FIGURE 11

N.E.R.C. JOB# 3274
CUSTOMER: NVL PO# DAAK70-80-C-0009
2.06 μ m WIDE BANDWIDTH DETECTOR ASSEMBLY
S/N 3274-5

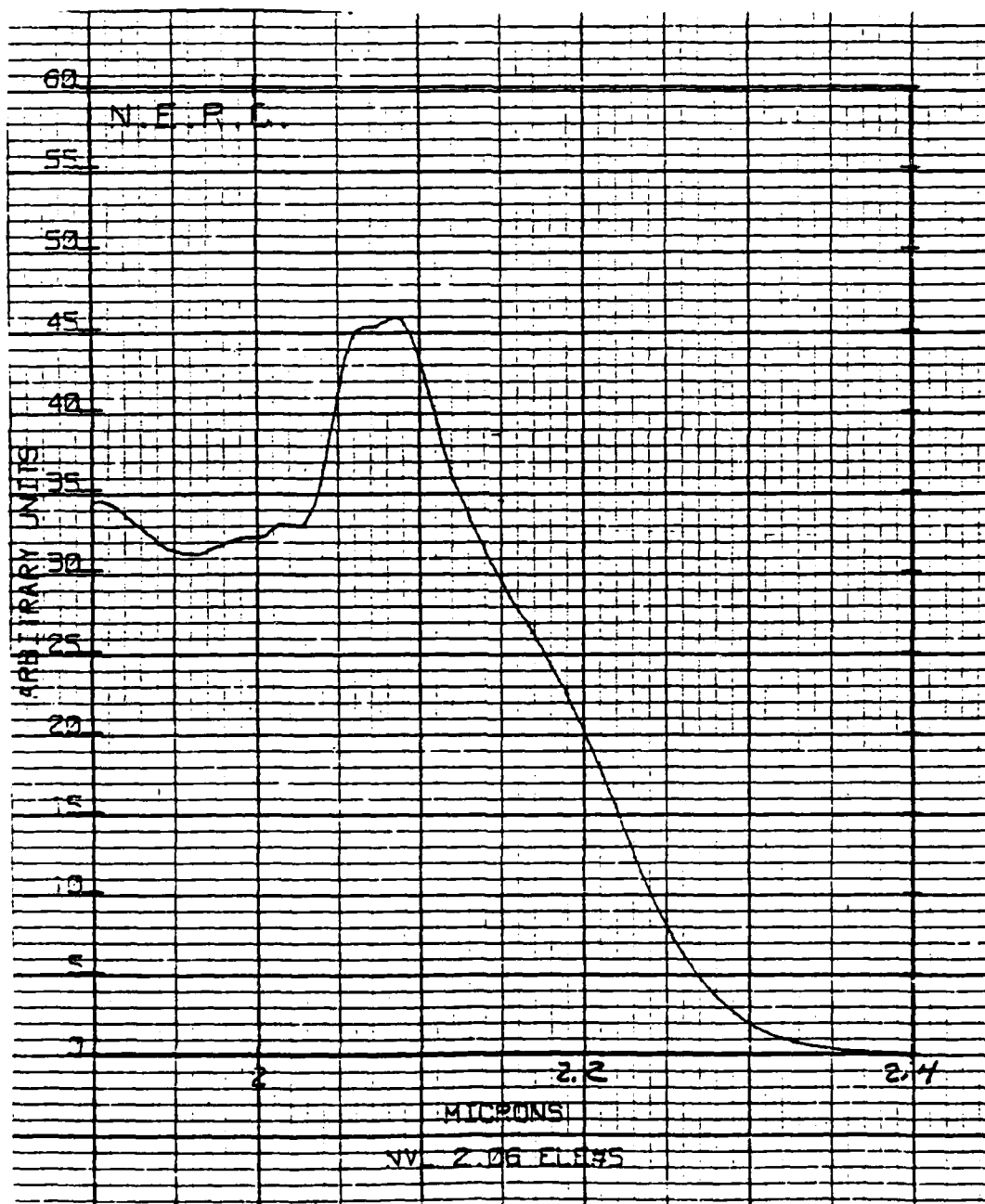


FIGURE 12

TABLE 4
BLACKBODY TO λ_{peak} CONVERSION FACTOR

G Factor 2.2 Micron Detector

$$G = \frac{\lambda_{\text{co}}}{hc} \cdot \frac{H_{\text{BB}}}{Q_0 - \lambda_{\text{co}}}$$

$$h = 6.6254 \times 10^{-34}$$

$$c = 3 \times 10^{10}$$

$$H_{\text{BB}} = 5.68 \text{ for } 1000^\circ\text{K Blackbody}$$

$$\lambda_{\text{co}} = 2.2 \text{ microns}$$

$$Q_0 = 1.52 \times 10^{20}$$

$$Q_0 \cdot \frac{Q_0 - \lambda_1}{Q_0 - \infty} = 1.52 \times 10^{20} \times 3.45 \times 10^{-2} = 5.244 \times 10^{18}$$

$$G = \frac{2.2 \times 10^{-4}}{(6.6254 \times 10^{-34})(3 \times 10^{10})} \cdot \frac{5.68}{5.244 \times 10^{18}}$$

$$= 1.1 \times 10^{19} \cdot 1.08 \times 10^{-18}$$

$$= 11.9$$

Both of the thermoelectric heat pumps were operated at a current of .75 Amps. A slightly lower power requirement was necessary for operation of the 4 stage cooler at 233°K.

During the measurements it was imperative to have complete shielding around the detector and heat sink. Extreme care was taken to eliminate ground loops. These measures became critical at the higher frequencies.

Conclusions and Recommendations

Although several critical technology issues remain to be solved, the major objective, detector performance, was achieved and the design goal exceeded by an order of magnitude. NERC demonstrated that $\text{Hg}_{1-x}\text{Cd}_x\text{Te}$ ($x = .475$) material can be grown with carrier concentrations on the order of $1 \times 10^{14}\text{cm}^{-3}$, and that this material can be processed into detectors of extremely high quality and performance.

It is beyond the scope of the present program to fully investigate the problems which effect yield, quality and reproducible fabrication. Areas in both crystal growth and wafer fabrication warrant further attention for any follow-on production of these devices.

This program demonstrated the feasibility of growing $\text{Hg}_{1-x}\text{Cd}_x\text{Te}$ ($x = .475$) with a carrier concentration approaching $1 \times 10^{14}\text{cm}^{-3}$. However, the growth related problems stated earlier must be addressed. This is summarized at (1) tighter control over alloy stoichiometry during solidification and (2) redesign of the pressure buttressing system to handle the high pressures encountered in $2.06\mu\text{m}$ material growth. NERC uses the Solid State Recrystallization process as a solution to these types of problems. It is imperative that the details of the process and tooling be optimized for future programs. To accomplish this, the approaches discussed below are proposed.

It is necessary to reduce the working stress on the pressurization system for a given buttressing pressure by increasing the wall thickness, decreasing the internal diameter, and selecting an alloy for the pressure vessel which has higher yield strength at elevated temperatures. Further modification involves decreasing the diameter of the crystal growth ampoule from 12.7mm to 10mm I.D. as well.

The required amount of excess Hg to be added to the growth ampoule during the loading stage which will yield the appropriate pressure over the liquid at a temperature T can be calculated from the equations given in reference 1. It is obvious that too much excess Hg will shift the partial pressure of Hg towards the higher free Hg pressure value and too little Hg will cause decomposition of the melt and change the stoichiometry. Also the extremely low carrier concentration requirement for this program poses an additional restraint whereby only slight Hg saturation during growth can be tolerated. The amount of excess Hg to be added therefore must be determined precisely by quenching several samples and investigating the saturation levels.

Advantages of performance enhancement such as in the area of extended frequency response beyond 10 Megahertz, remains to be used. Success will be contingent upon developing surface preparation tooling to establish wafer processing procedures to achieve detectors having the following characteristics:

- (1) Back of HCT and substrate must both be flat to $\frac{1}{2}$ micrometer.
- (2) The active area must be polished with its thickness uniform; rounding of the edges being permissible only over the contact areas.
- (3) Nondamaging polishing must be used since we cannot rely on heavy etching to remove surface damage.
- (4) Nondamaging materials handling procedures must be used.
- (5) The method should incorporate the possibility of using surface passivation on both the front and back faces.

The flat back and substrate are necessary in order to obtain a uniform detector thickness and a thin glue line. The first point is an obvious necessity; the second has two reasons: First, a thin glue line ensures minimum thermal resistance between the detector and the substrate. Second, unless the glue line is thin it is difficult to make the detector of uniform thickness; with a thick glue line the back of the detector is more likely to be non-parallel to the substrate and, since the glue line is of unknown thickness, it is difficult to know when the detector has been thinned to exactly 4 micrometers. A thin, uniform glue line is thus a prime necessity and it cannot be obtained without a flat surface on both HgCdTe and substrate. Not only do the surfaces of the detector have to be parallel and spaced 4 micrometers, but they have to be damage free. Therefore the normal polishing methods will not be useful. Present methods entail the use of heavy etching by Br in methanol to remove surface damage. This together with lapping on cloth laps produce a surface which is damage free but is curved. Flat damage free surfaces of soft material can be made using pitch and/or wax polishing laps. This technique requires additional development.

Non-damaging methods of handling the detector material are also necessary. All detector materials will be bonded to a temporary support substrate while fabrication operations are taking place. The supporting substrate would be removed after the HCT had been bonded to its final substrate. The method used would enable a passivation layer to be applied to the entire surface of the finished detector.

The detectors delivered were fabricated using standard methods, therefore, performance advantages anticipated through improved power dissipation designed into the 4 micron thick detectors was not realized. Specifically these areas are in the electrode design and use of thermal conductive epoxies.

From a systems point of view, the improvements mentioned above will push the detector knee out beyond 10 MHertz. This will eliminate the need for a video peaking amplifier, along with reductions in detectivity due to the increased noise associated with it. The detectivity increase will be a factor of 2 at 195°K. An increase the System Engineer cannot ignore.

DATE
FILME